JOURNAL OF SPACECRAFT AND ROCKETS
Vol. 39, No. 5, September–October 2002

Deployment Repeatability of a Space Telescope Reflector Petal

Johanne C. Heald* and Lee D. Peterson†
University of Colorado, Boulder, Colorado 80309-0429

An experimental investigation of the deployment repeatability of a reflector petal intended for a 3-m-diam space telescope is presented. The petal incorporates second-generation precision joint and hinge mechanisms that were designed for optical-level stability and hysteresis. The objective of the experiments was to determine the role of mechanism repeatability and structural kinematics in structural deployment repeatability. The deployment tests were performed in a thermally and mechanically isolated test chamber. A high-precision videometry system was used to measure the position of the petal tip in the two relevant degrees of freedom. The position of the petal for a total of 12 stow-and-deploy measurements are reported, from which the statistics of the petal position for any initial deployment are determined. The 95% confidence region for the deployed position is an ellipse 8.6 μm tall in the deploy/latch direction and 0.8 μm wide in the direction parallel to the hinge axis. The accuracy of the telescope petal's deployment is compared to that of a previously tested truss, and the telescope petal is found to have better repeatability in the hinge direction but less repeatability in the deploy/latch direction. The repeatability of the latch mechanism was found to account for fully the repeatability of the test article when projected through the kinematics of the structure. Indeed, the use of simple kinematics was conservative because it over-predicted the repeatability of the structure by 224%.

Nomenclature

a	=	length of base structure (see Fig. 11), m
b	=	length of reflector support (see Fig. 11), m
c	=	length of hinging structure (see Fig. 11), m
D	=	depth of structure, m
d_{microns}	=	displacement, μm
d_{pixels}	=	displacement, pixels
K	=	constant for videometry image calibration
L	=	length of structure, m
N	=	number of samples
P	=	confidence interval probability, %
S_x	=	sample standard deviation of x-direction displacements, m
$S_{\bar{x}}$	=	standard deviation of the mean of x-direction displacements, m
S_y	=	sample standard deviation of y-direction displacements, m
$S_{\bar{y}}$	=	standard deviation of the mean of y-direction displacements, m
t	=	time, s
$t_{\nu,P}$	=	Student-t estimator for confidence intervals
w	=	panel tip displacement in y direction (see Fig. 11), m
x	=	target horizontal axis (see Fig. 4), m
x_I	=	sample displacement in x direction, m
$\bar{x}$	=	mean displacement in x direction, m
y	=	target vertical axis (see Fig. 4), m
y_I	=	sample displacement in y direction, m
$\bar{y}$	=	mean displacement in y direction, m
z	=	axis perpendicular to target (see Fig. 4), m
α	=	angle of structure deployment (see Fig. 11), deg
θ	=	angle of petal deployment (see Fig. 4), deg
ν	=	statistical degrees of freedom
σ_k	=	error in calibration constant
σ_{pixels}	=	target displacement error, pixels
$\sigma_{\mu\text{m}}$	=	target displacement error, μm

Presented as Paper 2001-1302 at the 42nd Structures, Structural Dynamics, and Materials Conference; Seattle, WA, 16–19 April 2001; received 24 July 2001; revision received 2 January 2002; accepted for publication 22 February 2002.

*Graduate Research Assistant, Center for Aerospace Structures, Department of Aerospace Engineering Sciences; johanne.heald@colorado.edu. Student Member AIAA.

†Associate Professor, Center for Aerospace Structures, Department of Aerospace Engineering Sciences; lee.peterson@colorado.edu. Associate Fellow AIAA.

Introduction

THE Hubble Space Telescope has demonstrated the enormous benefit of space telescopes in astronomy, and it is sure to be followed by other spaceborne observatories with improved sensitivity and resolution. One planned future observatory of this type is the Next Generation Space Telescope (NGST). NGST is projected to have a primary mirror diameter over three times larger than that of Hubble, to gain greater sensitivity and, therefore, image more distant objects.[1] This primary mirror will not fit monolithically in any current launch vehicle; rather it must be segmented and deployed. This segmentation means that a fundamental technical challenge for imaging space telescopes will be to deploy and position the pieces of the primary mirror to within a small fraction of the wavelength of light it collects. The precision of this deployment is of the highest concern, because if the primary mirror is even marginally out of alignment, the telescope will not focus and will produce a distorted image.

Previous work by Warren and Peterson[2] and Warren et al.[3] on the deployment of support structures for optical space instruments has demonstrated that a conventional approach to the design of such purely passive structures will not achieve the nanometer-level precision desired in optical space telescope design. Specifically, it was found that a metering structure, when repeatedly deployed to its operational position, had a repeatability of a few microns at best. Warren and Peterson[2] then found that the deployment repeatability could be improved somewhat by applying small, impulsive loads that appeared to remove residual frictional stresses from the mechanisms and to allow the structure to settle into a somewhat more precise equilibrium zone.

In the intervening years, improvements in active optical positioning actuators effectively render this passive level of deployment repeatability well within the practical capability of any future active mirror control system. Several proprietary designs for such actuators

exist, all apparently sharing the common characteristic of having multiple stages of adjustment, with resolutions of nanometers and dynamic ranges (strokes) of many thousands of waves.

Why, then, is there still interest in deployment repeatability? Three factors are behind this interest. First, there are missions (such as an Earth-observing lidar) in which the demonstrated passive precision is nearly sufficient for the requirements of the mission, eliminating the need for actuators to position the optics. Second, if the passive deployment range of the structure is sufficiently tight, it may be possible to eliminate the coarse precision adjustment even for diffraction-limited infrared and visible telescopes such as NGST. This might save some of the cost, complexity, and mass in these systems. Third, and most important, it has been suggested[2] that deployment repeatability might be related to other significant structural response phenomena, such as postdeployment stability and spontaneous vibrations.

When the work of Warren et al.[3] was reported, it was unknown whether their measurements were unique to their test article, the Engineering Science Development Model (ESDM). The degree to which the observed imprecision was really the measurement error was also uncertain. Since then, the deployment repeatability of another structure consisting of a single boom, mirror and hinge, and latch mechanisms, the Precision Deployable Optical Structure (PDOS), was reported by Kozola et al.,[4] simultaneously with the initial presentation of the current study.[5] The repeatability of the PDOS structure was an order of magnitude less than that of the ESDM, with a repeatability on the order of tens of microns over a longer deployed structure. It is difficult to compare these results without some kind of normalization for the size of the structure. Therefore, the Warren et al.[3] results are still the most repeatable results available in the literature.

To see whether results comparable to these[2,3] can be achieved with a different structure, a new test article has been designed and constructed. The design of this test article is that of a flight-realizable metering structure for a 3-m-class deployable telescope. This test article is, therefore, a more mature design than the ESDM, which was never intended for flight but was a research test bed built with the aim of developing a micron-repeatable structure that would be suitable for spaceborne applications. Although the metering structure of the ESDM is more trusslike than that of the new test article, it deploys in a similar fashion, with the reflector support structure rotated about two precision hinges and latched into place.

The Warren et al. experiments showed[3] that the deployment repeatability of the ESDM could be correlated, to within 80%, with an imprecision in the latch projected through the kinematics of the truss. Thus, different kinematics should alter the deployment repeatability of the structure. In addition to the differing kinematics of the new test article and the ESDM, the two structures have differing mechanisms. The hinge joints of the two structures have similar, although not identical, designs. The latch joints, however, are quite different because the latch of the new test article was designed based on the principle of load path management. Essentially, load path management says that structural interfaces and joints should be designed to minimize the loss of total energy in internal inelastic mechanisms in the structure.[6,7] With the mechanism designed using this philosophy, the postdeployment stability of the structure should improve. Do other performance metrics, such as deployment repeatability, likewise improve? The present study experimentally explores the relationship between the kinematics and mechanisms of a structure and its deployment repeatability. The objective of the study is to determine whether mechanism repeatability can be used to predict the deployment repeatability of the full structure.

This paper is organized as follows: A description of the test article used in these experiments is given in the next section, followed by a description of the experimental apparatus and protocols that were used. Next, a characterization of the videometry system used to obtain displacement measurements is given. The results of the repeatability experiments are reported in the following section, and, in the next section, the results are compared to those obtained by Warren and Peterson[2] and Warren et al.[3] in their experiments with the ESDM. Finally, the latch mechanism on the test article is examined to determine its role in the test article's repeatability.

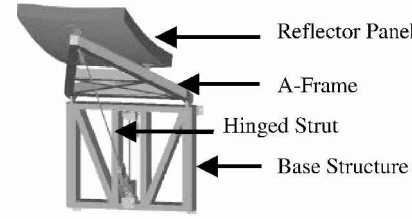

Fig. 1a Fully deployed panel that serves as the test article.

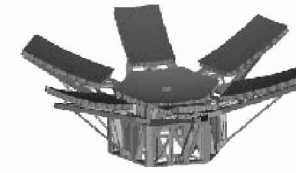

Fig. 1b Telescope, 3-m class, using six panels of the type shown in Fig. 1a.

Test Article

The test article used for the experiments of the present study is one petal of a seven-panel 3-m-class space telescope.[8] It is called the lidar prototype because one possible use of such a telescope is for the collection of atmospheric backscatter from a remote sensing lidar instrument. Figure 1a shows this single telescope petal standing alone, whereas Fig. 1b shows this single panel assembled with five others about a central mirror, as the full telescope would appear with all of its petals deployed. The average areal density of the mirror, including all hardware, and with six petals attached to a center body, is about 20 kg/m^2. This design is a significantly less massive than the Hubble primary mirror, which has an areal density of approximately 160 kg/m^2.

The main components of the test article are shown in Fig. 1a. The metering structure consists of a base structure (upright in Fig. 1a) and a supporting A-frame (inclined in Fig. 1a) that rotate about a common hinge line determined by two precision joints. A reflector panel is attached to this metering structure by three flexures. A strut attaches the outboard end of the A-frame to the base structure with precision hinges at either end. This strut controls the A-frame deployment.

In its stowed position, the A-frame and the base structure lie in a plane, with the strut lying against the A-frame. As the panel is deployed, the base of the strut moves away from the A-frame along a worm screw driven by a small motor. The A-frame, in turn, rotates about the two precision joints connecting it to the base structure. As the strut travels along the worm screw, it reaches the end of the base structure, and a latch is engaged to lock it in place. This latch drops the motor out of the load path. A full deployment rotates the reflector panel through approximately 75 deg. The metering structure in its deployed-and-latched configuration during manufacture is shown in Fig. 2.

The design of the hinge joint of the lidar prototype is detailed in Ref. 9; the design and fabrication of the latch for the lidar prototype can be found in Ref. 10. The latch is shown in Fig. 3 in its working position in the test article. It consists of a tapered bearing latch half-assembly, a locking mechanism assembly, and a lug latch half-assembly. To release the latch, the two flangelike lock fittings must be depressed, and the lug latch assembly must be moved forward over these two lock fittings by turning the worm-screw drive. This must be done manually because there is no motorized mechanism for depressing the lock fittings. Engaging the latch, in contrast, is a wholly automated process. The lug latch assembly is simply driven back over the locking mechanism by a motor that drives the worm-screw shaft. When the lug latch half has cleared the lock fittings, they snap into place, applying preload to the lug latch and forcing it to seat completely on the tapered bearing.

Experimental Apparatus and Protocol

In previous tests with other test articles, the environment proved to have a strong effect on the measured results. These experiments

Fig. 2 Lidar test article during manufacture.

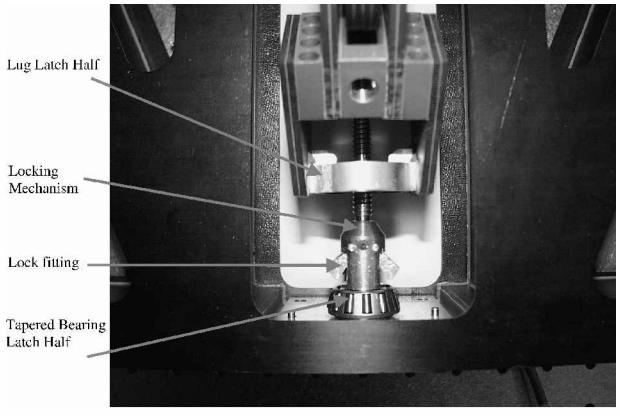

Fig. 3 Precision latch in lidar prototype test article.

were limited by an environmentally induced background vibration with an amplitude of 0.25–0.5 μm (Refs. 2 and 3). To reduce the effects of these disturbances, the lidar prototype was isolated from the environment by mounting it on an optics bench inside a thermal and acoustic stabilization chamber, where nanometer-level resolution has been previously achieved.[11] This chamber has a long-term thermal stability of 0.1°C and a short term stability of 0.01°C or better.

Figure 4 is a side view of the test article on the optics bench. The structural test article is anchored to the optics bench by four optical pedestals, at four symmetrically placed attachment points. The anchoring screws traverse from the bolt holes in the structure, through the pedestals, and directly into the optics bench, in an attempt to minimize the number of frictional linkages between the test article and the optics bench, which serves as reference for the measurements. A linear deployment actuator turns a worm-screw shaft located inside the base structure. This worm-screw shaft guides one end of the hinged strut along the base of the structure, in the *a* direction. The other end of the strut guides the outboard end of the panel

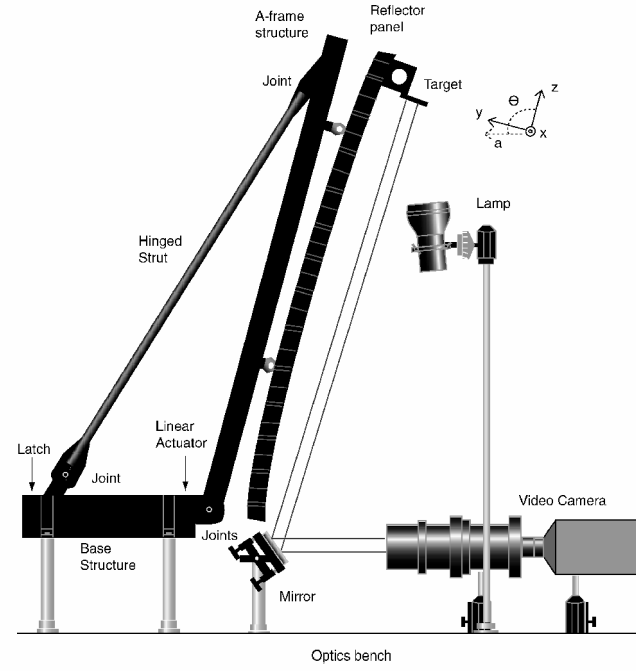

Fig. 4 Experimental apparatus for deployment repeatability experiments.

from its stowed position to its deployed position. Once the panel is in its deployed position, the strut engages the precision latch.

A videometry system was used to measure the position of the tip of the panel. A mount for the sensor target was attached to the panel with cyanoacrylate glue, and a target plate was attached to this mount with two screws. A 2.5 × 2.5 cm target was mounted on the target plate. The vertical and horizontal positions of this target, in its own plane, are measured by the videometry system and compared with earlier measurements to determine a shift in position. A mirror positioned at the base of the panel reflected the image of the target back to a video camera, which recorded the target position. The optical train was positioned and adjusted by hand; therefore, the misalignment of the mirror and camera with respect to the plane of the target is a possible source of error in the measurements. Other sensors were placed in the isolation chamber to monitor the temperature, humidity, atmospheric pressure, and local vibration environment during the deployments. Data collection from the videometry system took place at a rate of approximately 1 Hz.

The test protocol used in these tests is similar to that described in Ref. 2. It consists of a 24-h close-out period, in which the temperature and pressure inside the isolation chamber are allowed to equilibrate, followed by multiple deployments and stowings of the panel. A minimum of 2.5 h was allowed between each stow-and-deploy cycle, to permit thermal equilibration of the structure.

Because the precision latch used in the lidar prototype must be disengaged by hand, the isolation chamber had to be opened each time the panel was stowed. Care was taken during this period, approximately 3 min in duration, to allow very little change in the environmental conditions. The door was opened narrowly to inhibit air exchange with that outside the chamber. Other than the lamp needed to illuminate the target, no lights were used in the chamber, to reduce the amount of heat introduced into the environment. Nevertheless, the heat introduced by the experimenter during latch manipulation, as well as that given off by the motor during stow-and-deploycycles, must have added to the overall temperature of the chamber. Because this increase in temperature could not be avoided, it was monitored. The time between stow–deploy cycles was determined to provide sufficient thermal repeatability to within the resolution (40 nm) of the videometry system.

Characterization of the Videometry System

The videometry system used to measure the displacement of the test article between subsequent deployments measured the motion

of a target in the plane of the target and compared the shift in the image to a reference image to obtain displacement. The basic concept for this sensor system was described originally by Hinkle[12] and by Warren and Peterson.[2] The sensor determines relative position between two images, using a postprocessing shift-correlation analysis.

An essential capability of this sensor is that it retains the origin, or reference image, from deployment to deployment, even if the line of sight to the measurement target is interrupted. The origin is preserved by the stability of the optics and the targets. Other sensors that could have been used to take these measurements, such as interferometers, provide comparable resolution but do not measure position, only displacement with respect to an arbitrary origin. That origin is lost if the laser is interrupted. Other sensors, such as eddy-current probes, rely on the stability of their voltage power supplies for the long-term stability of their reference origin. The videometer used in the present study avoids these problems and is a low-cost solution for this type of measurement.

Because this measurement system was a somewhat unconventional, it was important to find out whether its measurements would be reliable. Therefore, an experiment was set up to evaluate those measurements against an interferometer.

The camera was set up in the configuration shown in Fig. 5. A flat target located on a displacement stage was moved in its own plane (vertically in Fig. 5) by a motor in controlled steps of approximately 300 nm and was illuminated by the lamp after every step. The camera then took a series of images that were averaged and used to determine the target's displacement. These displacement measurements were then compared with those taken simultaneously by a laser interferometer with known sources of error. The interferometer was positioned relative to the displacement stage such that it measured the position of the stage in the direction of motion. The camera can collect images to form a single averaged image at a rate of one per second.

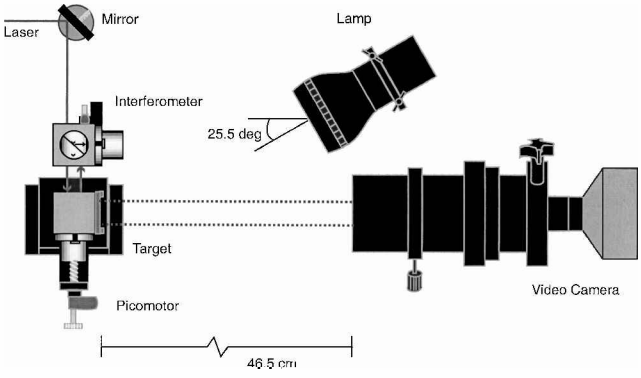

Fig. 5 Videometry verification testing apparatus.

Postprocessing of the images made it possible to measure shifts in the target with a resolution on the order of 0.001 pixels. The results (in pixels) of the image postprocessing are plotted against the displacement (in nanometers) measured by the interferometer as circles in Fig. 6. The image calibration line in Fig. 6 is the result of a calibration, in which the target was replaced by the American National Standards Institute/International Standards Organization Test Chart No. 2.[13] This test chart has different sizes of lines of known spacing in both the horizontal and vertical directions. From an image of this test chart, the number of nanometers represented by each pixel was found to be 9490 ± 500 nm. The image calibration line in Fig. 6 has, therefore, a zero intercept and a 9490 nm/pixel slope. The ± 500-nm error in this slope is represented by the dashed lines in Fig. 6. Note that the videometry data are quite accurate, although they clearly have a wandering bias with respect to the image calibration line. All of the deployment measurements reported in this paper are less than 1 pixel, and so a correcting algorithm using an estimator was applied to avoid underestimating the measurements. It is estimated that the accuracy of this algorithm is ± 0.006 pixels, or 100 nm.

Results and Discussion

The data from a typical stow-and-deploy cycle are shown in Fig. 7. The y direction referred to in Fig. 7 is the vertical axis of the target. That axis is tangent to the tip of the panel as it deploys. (See Fig. 4 for the orientation of the y axis.) The x motion in Fig. 7 represents the motion in the horizontal axis of the target, which is the direction out of the plane in Fig. 4. Because the deployment takes place in the direction of the angle θ of Fig. 4, motion in the x direction represents motion out of the plane of the deployment.

Figure 7 is a plot of the y position and x position of the tip target against time for a 2.5-h period (9000 s). Note the difference

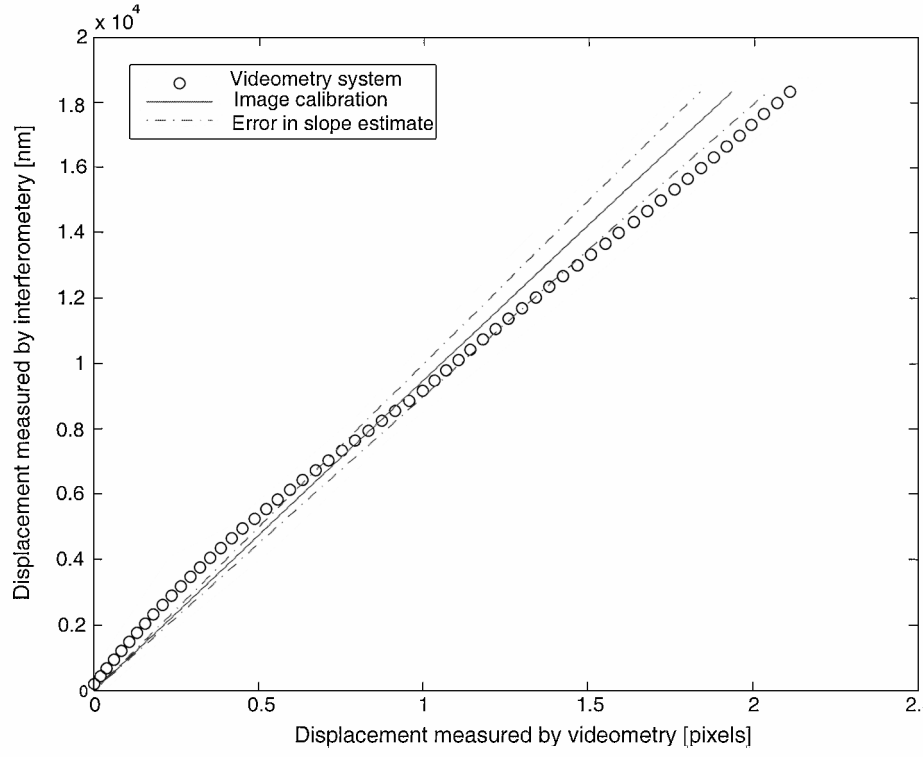

Fig. 6 Videometry system performance over 20 μm.

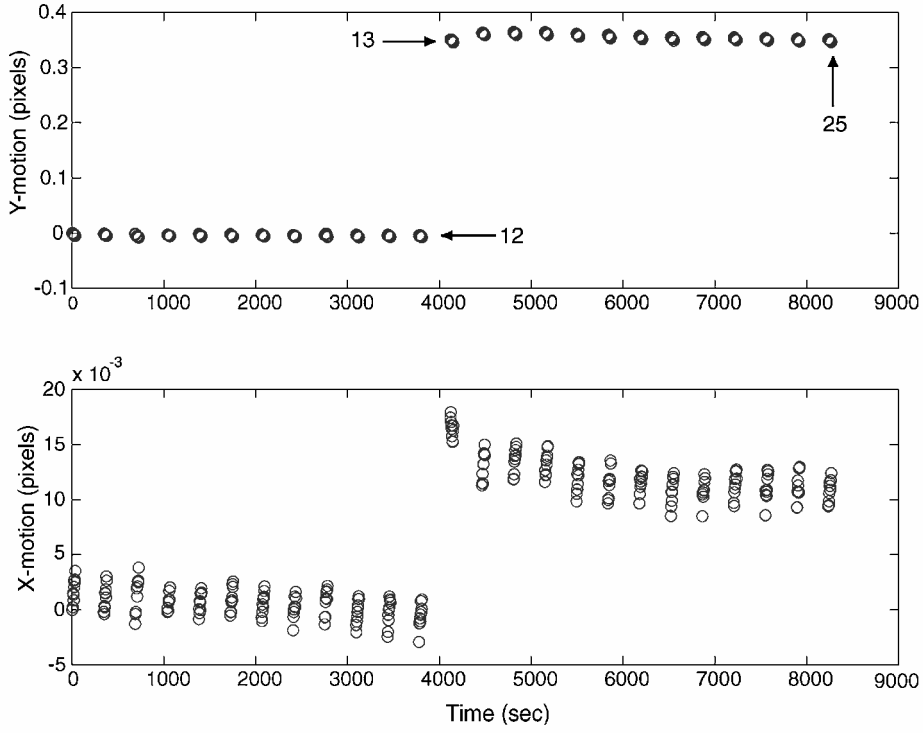

Fig. 7 Typical deployment time series for x and y target directions.

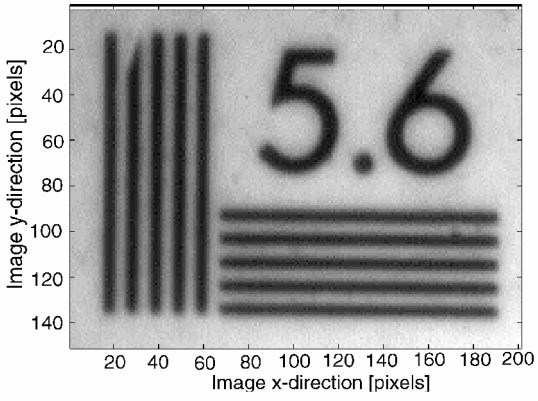

Fig. 8 Calibration image for deployment data.

in the scales of the ordinates. The position measurements are taken at 5 min intervals, at which time 10 images of the position target are captured. Note that the measurements are in units of pixels, as this is the unit the algorithm used to compute the shift in the image from one time step to the next.

Initially, the structure is in its deployed and latched state. The position measurements in Fig. 7 are consistent with this stationary state, although some small drift can be seen in the x direction. Then, just before 4000 s, between measurements 12 and 13, the latch was disengaged, the structure was stowed and it was then redeployed with reengagement of the latch. The measurements that follow $t = 4000$ s show a considerable change in the y position and a smaller change in the x position. Some settling of the position then occurs, probably due to the change in the thermal environment caused by opening the isolation chamber during the stow and deploy. At the end of the time sequence, the measurements settle to a final value. The change in deployed position is taken to be the difference in the position before the deployment (measurement 12, in this case) and at the end of the settling period (measurement 25). The change in deployed position is 0.3533 pixels in the y direction and 0.0138 pixels in the x direction.

It would be more meaningful to record the changes in position in micrometers rather than in pixels. The conversion from pixels to micrometers is made by using a calibrating image (Fig. 8) as the target. The same procedure that produced the image calibration line in Fig. 6 was used. The line spacing of this calibrating image is 5.6 lines/mm in both the x and y directions. Thus, the spacing of the lines in pixels was determined (0.098 ± 0.009 lines/pixel), and dividing this by the line spacing in micrometers leads to a conversion of 17.4 ± 0.2 μm/pixel. Therefore, for the stow-and-deploy sequence in Fig. 7, the change in deployed position is 6.15 ± 0.07 μm in the y direction and 0.240 ± 0.003 μm in the x direction, where the sited uncertainties are due to calibration only.

Table 1 Sources of experimental error

Source of error	Estimated value
Optical train misalignment	±0.0005 pixels
Thermal settling	±0.002 pixels
Videometry resolution	±0.001 pixels
Videometry accuracy	±0.006 pixels
Calibration error	±200 nm

The experimental error for each deployment measurement includes other uncertainties besides those due to the calibration. The misalignments of the optical train, thermal variation, and uncertainties introduced in processing the data must be included. The estimates of these error values are given in Table 1. These errors are combined by noting that

$$d_{\text{microns}} = K d_{\text{pixels}} \tag{1}$$

where d is the measured position, and, therefore,

$$\sigma_{\text{microns}} = \sqrt{(K\sigma_{\text{pixels}})^2 + (d_{\text{pixels}}\sigma_K)^2} \tag{2}$$

Using the maximum displacement in pixels, the maximum overall uncertainty of any deployment measurement is calculated, therefore, to be 120 nm.

Figure 9 is a scatter plot that displays the change in deployed position, which occurred during 12 such stow-and-deploy cycles. In other words, each circle represents the relative change in position from one deployment to the next (which is the difference between positions 12 and 25 in Fig. 7). The data were collected over a period of weeks. Outliers that were excluded from the analysis because of mechanical or data acquisition failures are not shown on this graph.

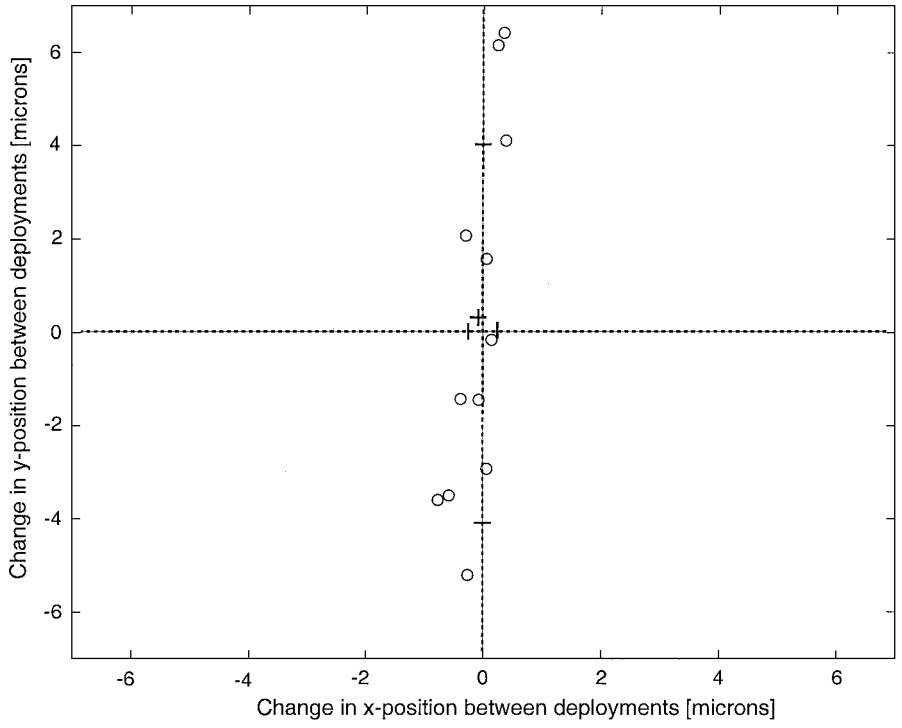

Fig. 9 Displacement data for 12 stow-and-deploy cycles.

Note that all of the data have now been converted from pixels to microns.

As the example plotted in Fig. 7 would lead us to expect, the changes in x position are much smaller than those in the y position. The mean of these 12 deployments does not quite fall at the origin. Rather, the mean is located at $x = -0.099$ μm and $y = 0.172$ μm, marked by the plus sign in Fig. 9. The sample standard deviation of the position measurements is calculated according to

$$S_x^2 = \frac{1}{N-1}\sum_{i=1}^{N}(x_i - \bar{x})^2 \tag{3}$$

$$S_y^2 = \frac{1}{N-1}\sum_{i=1}^{N}(y_i - \bar{y})^2 \tag{4}$$

where N is the total number of measurements and is equal to 12, the barred quantities are the means, and x_i and y_i are the individual measurements. Applying Eqs. (3) and (4) to the lidar prototype data results in an S_x of 0.367 μm and an S_y of 3.902 μm. These sample standard deviations can be used to determine the standard deviation of the mean of the deployed positions:

$$S_{\bar{x}} = S_x/\sqrt{N}, \qquad S_{\bar{y}} = S_y/\sqrt{N} \tag{5}$$

The standard deviations of the deployed position means are, therefore, 0.1 μm in the x direction and 1.1 μm in the y direction. Because these standard deviations are greater than the means themselves, it is concluded that there is no discernable positive or negative bias in the deployment repeatability.

Comparison with ESDM Results

To compare the results of the lidar prototype with the ESDM results, it is necessary to estimate statistically the infinite sample statistics for each from the finite size sample sets involved. The set for the lidar prototype has 12 measurements, and the ESDM results have 40 measurements. To compare the infinite statistics of these data sets of finite sample size, a statistical confidence interval is determined for each set of results. This is done by assuming that the distribution of measurements x is a normal distribution with a mean value $\bar{x}$; then the uncertainty of a single sample x_i can be determined from

$$x_i = \bar{x} \pm t_{\nu,P} S_x(P\%) \tag{6}$$

with a confidence probability of $P\%$. In Eq. (6), ν are the degrees of freedom in the standard deviation, and t is the Student-t estimator for the confidence interval of finite statistics. The Student-t estimator corrects the Gaussian probability interval to obtain a larger interval that accounts for the finite size of the sample set. The choice of confidence interval $P\%$ is somewhat arbitrary. Following a common convention, the 95% probability confidence interval was chosen. Reference 14 lists a value of 2.201 for $t_{11,95\%}$. When Eq. (6) is applied, the repeatability data for the lidar prototype have a 95% confidence interval of 8.588 μm in the y direction and 0.808 μm in the x direction.

These results can be compared with those obtained on the ESDM. The standard deviation of the deployment repeatability is given in Ref. 2 for both a left and a right tip target. There were 40 measurements in those sample sets, not 12, and so the Student-t corrector is different. The right tip target had S_x of 0.83 and S_y of 1.73, whereas the left tip target had S_x of 1.47 and S_y of 1.47. The standard deviations are multiplied by $t_{40,95\%} = 2.021$ to obtain the 95% confidence intervals.

The results are compared graphically in Fig. 10. In Fig. 10, the hinge–axis direction in both the ESDM and the lidar prototype are in the horizontal direction on the page. Note that, whereas the lidar repeatability results in Fig. 9 do not scatter into a perfectly elliptical shape, an elliptical confidence interval has been drawn in Fig. 10 to facilitate the comparison with the ESDM. The ellipses of Fig. 10 show that, whereas the deployment repeatability of the lidar prototype is better than that of the ESDM in the direction of the hinge axis (x direction), it is worse than that of the ESDM in direction of the angle of the deployment (y direction).

This comparison of the absolute repeatability of the two structures is a good way of evaluating their relative performance, but it presents an incomplete picture. The difference in the kinematics of the linkages, that is, the lengths, of the two designs is not taken into account. These differences lead to different sensitivities of the tip position to position errors in the latch mechanisms. The kinematic links in the two structures are shown in Fig. 11 and Table 2. The lidar prototype in Fig. 11 is in the same orientation as it was in Fig. 4.

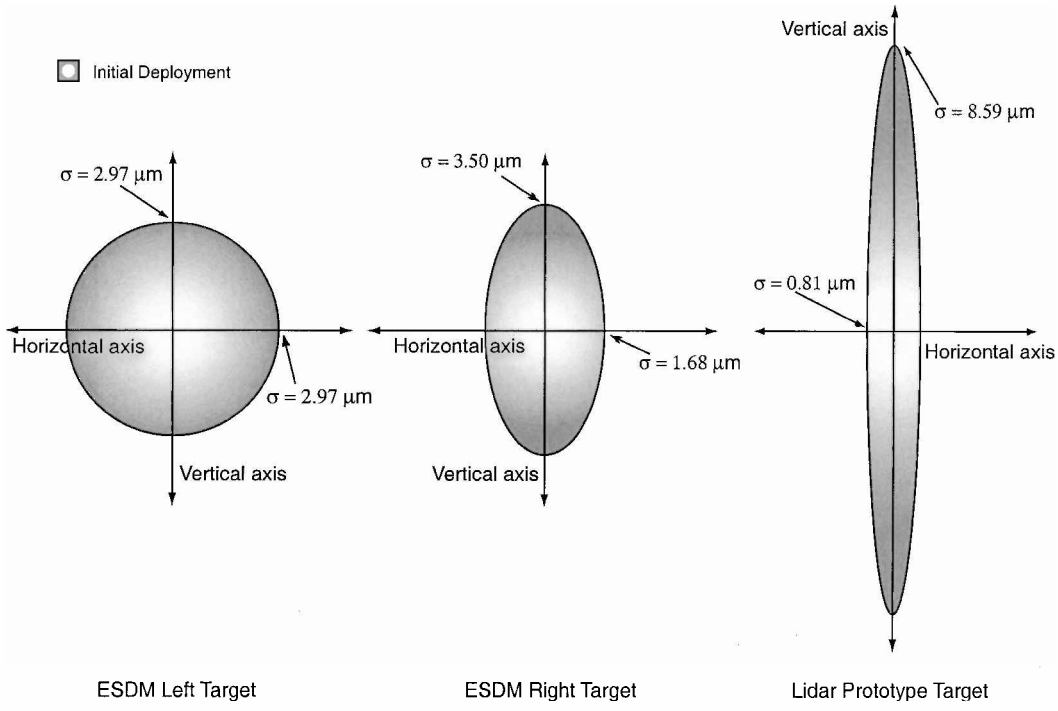

Fig. 10 Comparison of raw confidence intervals for lidar prototype and ESDM.

(Note that the length a in Fig. 11 is in the a direction indicated in Fig. 4 and that α in Fig. 11 measures the angle between the base structure and the hinged structure at the location of the latch. Note also that the location of the latch in the two structures is different.) The characteristics of the ESDM as compared to the lidar prototype are presented in Table 3. Note that the ESDM has a larger length-to-depth (L/D) ratio than the lidar prototype. Table 3 also lists, for both structures, the nominal values of a, b, c, and α, as shown in Fig. 11. The kinematic differences between the two structures result in tip positions that have different sensitivities to different errors.

As a result, the following normalization procedure is proposed: the ratio of the sensitivities of the tip position to the latch position is used as a normalizing factor between the two structures. In Fig. 11, the length w represents displacement in the deployment direction of the structure. The latches for the lidar prototype and the ESDM are located on the linkage a, at the joint indicated by the angle α. The sensitivity of a change in w with respect to a change in the position of the latch can be found by differentiating the expression for w with respect to the variable of interest.

The derivatives with respect to changes in b and c in Table 2 indicate the sensitivity of the tip displacement to off-axis motion of the latch. The geometry of the lidar prototype reduces this sensitivity with respect to the ESDM. However, there is a tradeoff: the sensitivity of the tip to the axial position of the latch (derivative with respect to a in both cases) is higher for the lidar prototype than for the ESDM. Therefore, errors in the direction of latch closure will be magnified by the kinematics of the lidar prototype.

To normalize for the different kinematics, ratios of the sensitivities are formed as normalizing factors. Because the direction of latch closure is the one in which the most variation in the lidar prototype is expected, this sensitivity is selected, and a normalization factor of $(1.05\ \mu\text{m}/\mu\text{m})/(1.49\ \mu\text{m}/\mu\text{m}) = 0.70$ is formed. Thus, the lidar prototype confidence interval of 8.59 μm is comparable to a confidence interval of $8.59\ \mu\text{m} \times 0.70 = 6.05\ \mu\text{m}$ for a structure with ESDM-like kinematics. Note that this confidence interval is still twice as big as the 95% confidence interval of the ESDM results shown in Fig. 10. Based on this difference, we must acknowledge that something beyond the kinematic difference of the two structures has influenced the deployment repeatability results.

In all probability, that something is the repeatability of the latch itself. Repeated deployments of the test article demonstrated vividly that the "goodness," or accuracy, of the latch fit was extremely

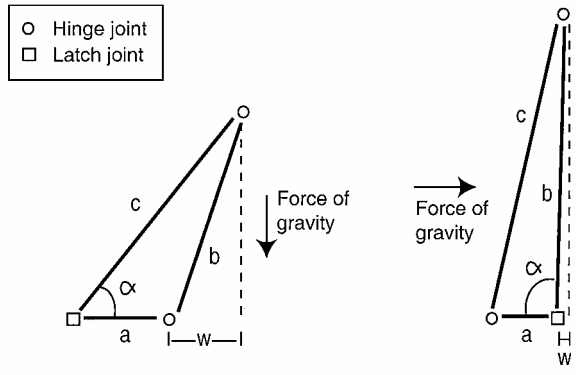

Fig. 11 Kinematic sensitivity of the lidar prototype and ESDM.

Table 2 Kinematic sensitivity of the lidar prototype and ESDM

Lidar prototype	ESDM
$w = c\sin(90^\circ - \alpha) - a$	$w = b\cos(180^\circ - \alpha)$
$\frac{dw}{da} = -1.49$	$\frac{dw}{da} = -1.05$
$\frac{dw}{dc} = +2.37$	$\frac{dw}{db} = -4.32$

sensitive to the manufacture and assembly of the latch parts. Several adjustments were made on the assembled structure, and the locking mechanism underwent some remachining, even though the parts had been manufactured within the tolerances of ± 0.000254 m (dimensional) and ± 0.5 deg (angular) stipulated in the original design.[10] The data presented were obtained after all adjustments had been made. Nevertheless, it was observed that the latch did not perform entirely as anticipated. In particular, the right flange lock fitting did not extend as fully as the left-side flange. This asymmetry may have altered the amount of preload applied to the lug half of the latch and may, in part, account for the decreased repeatability compared with that of the ESDM. Note also that the gravity loading, as shown in Fig. 11, is different for the two structures and has a different effect on the latch. For the lidar prototype, the gravity loading

Table 3 Comparison of the lidar prototype and ESDM test articles

Test article	Material	Design	L/D	a, m	b, m	c, m	α, deg
Lidar	K135U/954-3 plated, layup [0/−60/60/ −60/0]	Strut deployment	1.54	0.41	0.78	0.97	50.9
ESDM	Graphite-epoxy tubes, layup unidirectional	Trusslike deployment	3.44	0.26	1.10	1.14	93.0

Table 4 Lidar prototype latch repeatability data

Cycle	Δx, μm, ± 0.1 μm	Δa, μm, ± 0.1 μm
	Data set 1	
1	7.7	1.0
2	1.3	−0.1
3	−3.3	2.9
4	−0.4	1.1
	Data set 2	
1	0.3	4.2
2	−1.3	−6.0
3	3.9	3.2
4	−1.8	−3.0
5	1.2	−3.2
	Data set 3	
1	1.8	3.7
2	−6.2	−9.6
3	3.1	13.5

tends to open the latch; for the ESDM, the gravity loading tends to close the latch. Thus, gravity unfavorably biases the preload of the lidar prototype latch with respect to the ESDM latch. Although the force of gravity itself should not affect the repeatability of the structures (because the orientation of the test article was constant during all of the deployment experiments), it may indirectly affect the results because of the differing magnitude and orientation of the preload vector that gravity applies to the mechanisms. Changing the setup of the lidar prototype so that its orientation would match that of the ESDM was considered for these experiments, but was found to be inadvisable because it would require a reorientation of the optics bench as well.

Examination of the Lidar Prototype Latch

Previous work[3] determined that the uncertainty in the deployed position of the ESDM could be correlated to within 80%, with an imprecision in the latch projected through the kinematics of the truss. Is it possible to account for the uncertainty in the deployed position of the lidar prototype in the same way? To test the hypothesis that an imprecision in the latch is responsible for the deployment uncertainty of the structure, an experiment was conducted to test the repeatability of the latch itself in situ.

The same apparatus shown in Fig. 4 was used for the latch repeatability tests, although, in this case, two targets were used: One was fixed to the underside of the lidar prototype base structure, whereas the other was mounted to the traveling part of the latch. (A special bracket had to be designed and fixed to the latch to allow this.) The mirror was repositioned under the latch, so that when the structure is in the deployed-and-latched position, both of the targets are in the camera field of view. See Fig. 12 for one such image taken by the camera. Thus, the position of the traveling part of the latch can be compared with the position of the part that remains fixed to the lidar prototype.

The lidar prototype was cycled through several stow-and-deploy sequences as before, only this time, it was the position of the latch that was measured. Three sets of data were taken, as shown in Table 4, with each set containing a number of stow-and-deploy cycles. Very little drift of the measured position was detected in the data. Table 4 lists the changes in position (in microns) for each of the stow-and-deploy cycle. Note that x is the same direction used in the earlier experiments but that the y direction has been replaced

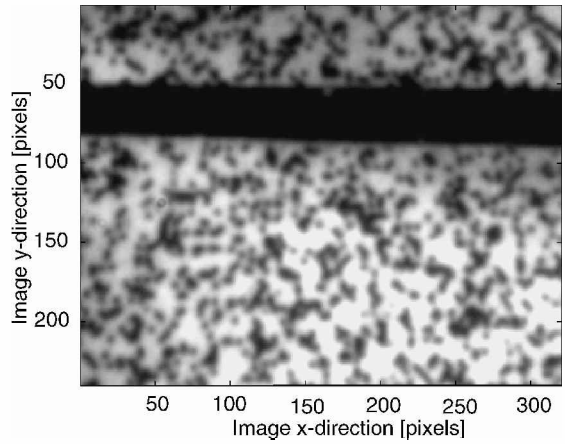

Fig. 12 Target image for latch repeatability experiments.

with the a direction (see Fig. 4 for the orientation of these vectors). The change in position is taken to be the difference of the mean sampled position immediately before the stow and deploy and the mean sampled position immediately after the stow and deploy. This is slightly different from the way the repeatability was measured in the earlier repeatability tests, in which the final position was not the one immediately after the stow and deploy but at the end of a 1.5-h postdeployment settling period. The postdeployment settling accounts for the thermal changes introduced by opening the test chamber during the stow and deploy. Because there seemed to be no discernable drift in the latch position after the stow and deploy, a postdeployment settling period was deemed unnecessary in this case.

The mean of the measurements in the x and a directions are 0.55 and 0.64 μm, respectively. The sample standard deviations are $S_x = 3.59$ μm and $S_a = 5.85$ μm. Because 12 sample points were used to calculate these measurements, the 95% confidence interval can be found using Eq. (6) and the same value of $t_{11,95\%}$ (Ref. 11) as before, producing 95% confidence intervals of 7.90 μm in x and 12.89 μm in a.

The a direction is the axis along which the mating of the two halves of the latch takes place. This is the deployment direction and the direction of the application of the preload. Thus, a lack of repeatability of the preload application, as discussed earlier, would account for the lack of repeatability of the latch in this direction. Another factor that might influence the mechanism in this direction is the misalignment of the two halves of the latch. From the sensitivity analysis in Table 2, $\partial w/\partial a = -1.49$. Thus, by applying simple kinematics, the 12.89-μm confidence interval at the latch in the a direction produces a confidence interval of 19.21 μm at the tip of the structure. This quite surpasses the confidence interval of 8.588 μm that was actually measured at the tip, and overpredicts it by 224%. In fact, the difference in the size of the confidence intervals implies that the mechanics of the structure itself are reducing the uncertainty that one would expect from a simple kinematic projection of the latch uncertainty. In other words, repeatability of the mechanisms may not be the only factor in the repeatability of the structure because the redundancy of the structure itself must also be taken into account.

The x direction of the latch is perpendicular to the mating direction, in the plane of the table. The latch is very much constrained in this direction, and it is unlikely that the measured imprecision is due to translation of the latch. Rather, it seems much more likely that the displacements measured in this direction are actually rotations of the latch about the a axis, projected onto the x direction because neither part of the latch is well constrained against such a rotation. Because of the two hinges connecting the A-frame of the structure to the base, the rotation of the latch (and, therefore, the strut connecting the base to the A-frame) has little effect on the repeatability of the structure. However, too much rotation could cause a misalignment of the latching halves, which would result in greater a-direction imprecision.

Conclusions

This paper reports on experiments that determined the structural deployment repeatability of a deployable space telescope reflector panel. In particular, these experiments measured the change in the panel's tip position as the test article went through multiple stow-and-deploy cycles. The tip position was measured in both the direction of the deployment (the latch–unlatch direction of the deployment latch) and in the hinge–axis direction of the structure. The repeatability of the lidar prototype is comparable to that of the most precise structure of similar size measured to date, the ESDM. Thus, the ESDM is not a unique structure in achieving high deployment repeatability. The deployment repeatability in the hinge–axis direction of the lidar prototype was significantly better than that achieved on the ESDM. However, the level of deployment imprecision in the latch–unlatch direction was twice that of the ESDM results. The latch–unlatch direction is the most critical for the performance of the telescope, and so repeatability in this direction is of greater concern. When a normalization procedure was applied to take the kinematic differences between the two structures into account, the repeatability of the lidar prototype was still not as good in the deployment direction as that of the ESDM.

Examination of the lidar prototype latch showed that the uncertainty of the position of the latch fully accounted for the uncertainty in position measured at the tip of the panel. The ESDM uncertainty has been correlated to within 80% with the uncertainty in its latch. Thus, the repeatability of the latching mechanism dominates the repeatability of both of these structures. Consequently, an appropriate method of predicting the repeatability of these structures would be the projection of the repeatability of all of the mechanisms (measured with the proper vectoral loads applied) through the kinematics of the structures. For some structures, this prediction may be conservative because it does not take the redundancy of the structure into account. The lidar prototype is one such structure because the uncertainty predicted by applying the kinematics of the structure to the latch repeatability results exceeded the uncertainty that was actually measured by 224%.

Acknowledgments

This research was supported by NASA Cooperative Agreement NCC1-281 through NASA Langley Research Center, with Mark Lake as Technical Monitor, and by NASA Cooperative Agreement NCC9-65 through NASA Johnson Space Center, with Carlos Parra as Technical Monitor. The help given by Mark Lake and Jason Hinkle configuring the test article and interpreting the results is gratefully acknowledged.

References

[1]Bely, P., "The NGST 'Yardstick Mission'," *The Next Generation Space Telescope, Science Drivers and Technological Challenges: Proceedings of the 34th Liege International Astrophysics Colloquium*, European Space Agency, Liege, Belgium, 1998, pp. 159–166.

[2]Warren, P. A., and Peterson, L. D., "Sub-Micron Non-Linear Shape Mechanics of Precision Deployable Structures," Ph.D. Dissertation, Center for Aerospace Structures, CU-CAS-96-18, Univ. of Colorado, Boulder, CO, July 1996.

[3]Warren, P. A., Peterson, L. D., and Hinkle, J. D., "Submicron Mechanical Stability of a Prototype Deployable Space Telescope Support Structure," *Journal of Spacecraft and Rockets*, Vol. 36, No. 5, 1999, pp. 765–771.

[4]Kozola, B., Erwin, R., Robertson, L., Griffin, S., and Powers, M., "Experimental Characterization of Deployment Repeatability for Optical-Precision Space Structures," AIAA Paper 2001-1267, April 2001.

[5]Heald, J. C., and Peterson, L. D., "Deployment Repeatability of a Space Telescope Reflector Petal," AIAA Paper 2001-1302, April 2001.

[6]Hachkowski, M. R., Peterson, L. D., and Lake, M. S., "Load Path Management Design Theory for Precision Deployable Joints," AIAA Paper 2000-1364, April 2000.

[7]Lake, M. S., and Hachkowski, M. R., "Design of Mechanisms for Deployable, Optical Instruments: Guidelines for Reducing Hysteresis," NASA TM-2000-2 10089, March 2000.

[8]Lake, M. S., Phelps, J. E., Dyer, J. E., Caudle, D. A., Tam, A., Escobedo, J., and Kasl, E. P., "A Deployable Primary Mirror for Space Telescopes," *Proceedings of the Advanced Telescope Design, Fabrication, and Control Conference*, Society of Photo-Optical Instrumentation Engineers, SPIE Proceedings, Vol. 3785, Bellingham, WA, 1999, pp. 14–25.

[9]Lake, M. S., Warren, P. A., and Peterson, L. D., "Revolute Joint with Linear Load-Displacement Response for a Deployable Lidar Telescope," AIAA Paper 96-1500, April 1996.

[10]Phelps, J. E., "Fabrication and Assembly of High-Precision Hinge and Latch Joints for Deployable Optical Instruments," NASA CR-1999-209117, March 1999.

[11]Hardaway, L. M. R., and Peterson, L. D., "Stability and Mechanics of Precision Deployable Structures Under Nanometer Deformation," Ph.D. Dissertation, Center for Aerospace Structures, CU-CAS-00-05, Univ. of Colorado, Boulder, CO, Feb. 2000.

[12]Hinkle, J. D., "A Micron-Precision Metrology System for Measuring Structural Geometric Repeatability" M.S. Thesis, Center for Aerospace Structures, CU-CAS-95-16, Univ. of Colorado, Boulder, CO, Aug. 1995.

[13]"Micrographics—ISO Resolution Test Chart No. 2—Description and Use," American National Standards Inst. Rept., ANSI/ISO 3334-1991, Association for Information and Image Management, Silver Spring, MD, 1991.

[14]Figliola, R. S., and Beasley, D. E., *Theory and Design for Mechanical Measurements*, 2nd ed., Wiley, New York, 1995, pp. 138, 139.

M. P. Nemeth
Associate Editor